CHAPTER 21

SHOALING OF FINITE-AMPLITUDE WAVES ON PLANE BEACHES

Robert K -C Chan[1]
Robert L Street,[1] M ASCE

ABSTRACT

This work focuses on the shoaling of large water waves with particular application to storm-generated waves and tsunamis The specific objective is the exact simulation on a digital computer of finite-amplitude waves advancing on a beach of constant slope

The study is based on the simulation technique called SUMMAC (the Stanford-University-Modified Marker-And-Cell Method) The flow field is represented by a rectangular mesh of cells and by a line of hypothetical particles which defines the free surface Based on the Navier-Stokes equations, finite-difference equations were derived so that the entire flow configuration could be advanced through a finite increment of time The pressure and velocity components are used directly as the dependent variables Through extensive analyses and numerical experiments, this scheme was found to be computationally stable if the cell size and the time increment are properly selected

As a specific example, the dynamics of a solitary wave passing from a zone of constant depth onto a sloping beach were simulated Primary attention was focused on the details of the water particle motions and the changes in the amplitude and shape of the wave as it climbed the slope The computed results are compared with the experiments with good agreement

INTRODUCTION

The motion of water waves whose amplitudes are appreciable in relation to the water depth is nonlinear in nature (Stoker, 1957) Consequently the linearized theory (Lamb, 1945) does not provide adequate physical description of waves in the shallow-water zones Most of the existing nonlinear analytical theories deal with a steady-state solution (See, e g , Laitone,1960, Dean, 1965, Monkmeyer and Kutzback, 1965) However, in shallow water the primary interest is in the transient aspect of the wave processes It is quite difficult to treat time-dependent problems of this kind without recourse to computational methods

At present several numerical methods are available for computing waves in shallow water and nonlinear terms are included to some extent (See, Street, et al , 1970, for a detailed summary) These methods retain in their governing equations the terms representing the kinetic energy of the vertical motion to varying degrees of accuracy Only

[1]Department of Civil Engineering, Stanford University, Stanford, California 94305

one space variable, namely x , is involved Vertical variation of the fluid variables has been eliminated by integration or a series expansion approach and use of boundary conditions These approximate theories generally produce good results for long waves of small but finite amplitude-to-depth ratio However, more must be known about the internal distribution of pressure and velocity which must be incorporated in the governing equations of motion if one wishes to study waves of considerable amplitude

Chan and Street (1970a) proposed a computing technique for analyzing two-dimensional finite-amplitude water waves under transient conditions The method, called SUMMAC, is a modified version of the Marker-And-Cell method (MAC) which was originally developed by Welch, et al (1966) The essence of the modifications consists of a rigorous application of the pressure boundary condition at the free surface and of an extrapolation of velocity components from the fluid interior so that inaccuracy in shifting the free surface is kept at a minimum

Thus, Chan and Street (1970a) outlined the basic features of SUMMAC and established its viability as an engineering research tool The present work summarizes the earlier study, presents some essential new concepts and features, and finally, in giving a means of treating sloping beach problems, greatly broadens the realms of usage of MAC-type programs

THE SUMMAC METHOD

The presently implemented SUMMAC is designed for simulating the unsteady motion of water waves in two space dimensions The fluid is regarded as incompressible and the effect of viscosity is considered to be negligible

To set up a computing network, the entire flow field is covered with a rectangular mesh of cells, each of dimensions δx and δy The center of each cell is numbered by the indices i and j , with i counting the columns in the x-direction and j counting the rows in the y-direction of a fixed Cartesian coordinate system (Fig 1) The field-variable values describing the flow are directly associated with these cells (Welch, et al , 1966) The fluid velocity components u and v and the pressure p are used as the dependent variables while the independent variables are x and y , the Cartesian space coordinates, and the time variable t

In addition, there is a line of marker particles whose sole purpose is to indicate where the free surface is located The marker-and-cell system provides an instantaneous representation of the flow field for any particular time during the evolution of the dynamics

By neglecting viscosity, we can reduce the Navier-Stokes equations for an incompressible fluid to

$$\frac{\partial u}{\partial t} + u \frac{\partial u}{\partial x} + v \frac{\partial u}{\partial y} = - \frac{\partial p}{\partial x} + g_x \ , \qquad (1)$$

$$\frac{\partial v}{\partial t} + u \frac{\partial v}{\partial x} + v \frac{\partial v}{\partial y} = - \frac{\partial p}{\partial y} + g_y \qquad (2)$$

Here g_x and g_y are the components of gravity acceleration All variables are dimensionless The continuity equation is

$$\frac{\partial u}{\partial x} + \frac{\partial v}{\partial y} = 0 \qquad (3)$$

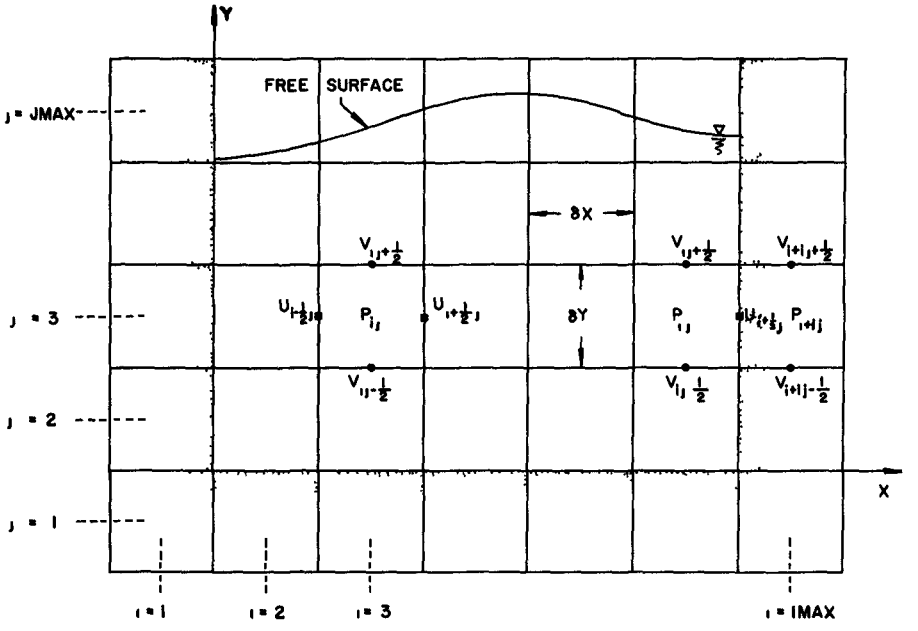

Fig 1 Cell Setup and Position of Variables

On the surface of a vertical impermeable wall, the boundary conditions are

$$u = 0 , \quad \frac{\partial v}{\partial x} = 0 \quad \text{and} \quad \frac{\partial p}{\partial x} = g_x \qquad (4)$$

Similar procedures can be followed to derive the boundary conditions for a horizontal solid boundary

$$v = 0 \ , \quad \frac{\partial u}{\partial y} = 0 \quad \text{and} \quad \frac{\partial p}{\partial y} = g_y \tag{5}$$

For incompressible fluids with very low viscosity, such as water, it is sufficiently accurate to use the single condition on the free surface

$$p = p_a(x,t) \ , \tag{6}$$

where p_a is the externally applied pressure at the free surface (Chan and Street, 1970a)

A finite-difference scheme can be derived from Eqs (1), (2) and (3) for cell (i,j) in Fig 1 as follows

$$u^{n+1}_{i+\frac{1}{2}j} = u^{*}_{i+\frac{1}{2}j} + \delta t \cdot g_x + \frac{\delta t}{\delta x}\left(p_{ij} - p_{i+1j}\right) \ , \tag{7}$$

$$v^{n+1}_{ij+\frac{1}{2}} = v^{*}_{ij+\frac{1}{2}} + \delta t \cdot g_y + \frac{\delta t}{\delta y}\left(p_{ij} - p_{ij+1}\right) \ , \tag{8}$$

$$D^{n+1}_{ij} \equiv \frac{u^{n+1}_{i+\frac{1}{2}j} - u^{n+1}_{i-\frac{1}{2}j}}{\delta x} + \frac{v^{n+1}_{ij+\frac{1}{2}} - v^{n+1}_{ij-\frac{1}{2}}}{\delta y} = 0 \ , \tag{9}$$

where D_{ij} is the velocity divergence, u^* and v^* are contributions to u^{n+1}_{ij} and v^{n+1}, respectively, by pure convection Variables with the superscript n+1 are related to the n+1th time step while those lacking a superscript are evaluated at the nth step If the original MAC scheme is used, u^* and v^* are evaluated by

$$u^{*}_{i+\frac{1}{2}j} = u_{i+\frac{1}{2}j} + \delta t \left[\frac{u^2_{ij} - u^2_{i+1j}}{\delta x} + \frac{(uv)_{i+\frac{1}{2}j-\frac{1}{2}} - (uv)_{i+\frac{1}{2}j+\frac{1}{2}}}{\delta y} \right], \tag{10}$$

$$v^{*}_{ij+\frac{1}{2}} = v_{ij+\frac{1}{2}} + \delta t \left[\frac{(uv)_{i-\frac{1}{2}j+\frac{1}{2}} - (uv)_{i+\frac{1}{2}j+\frac{1}{2}}}{\delta x} + \frac{v^2_{ij} - v^2_{ij+1}}{\delta y} \right] \tag{11}$$

Substituting Eqs (7) and (8) into Eq (9) and requiring $D^{n+1}_{ij} = 0$ lead to the pressure equation

$$p_{ij} = \frac{1}{Z}\left(\frac{p_{i+1j} + p_{i-1j}}{\delta x^2} + \frac{p_{ij+1} + p_{ij-1}}{\delta y^2} + R_{ij} \right), \tag{12}$$

where

$$Z \equiv 2\left(\frac{1}{\delta x^2} + \frac{1}{\delta y^2}\right) \quad , \tag{13}$$

$$R_{ij} \equiv -\frac{1}{\delta t}\left[\frac{u^*_{i+\frac{1}{2},j} - u^*_{i-\frac{1}{2},j}}{\delta x} + \frac{v^*_{i,j+\frac{1}{2}} - v^*_{i,j-\frac{1}{2}}}{\delta y}\right] \tag{14}$$

Near the free surface "irregular stars" (Fig 2) must be used to derive a special equation for pressure so that, in the discrete sense, the free surface condition [Eq (6)] is applied at the exact location of the surface and not in a nearby cell center where p is normally defined Let η_1 , η_2 , η_3 , η_4 be the lengths of the four legs of the irregular star (Fig 2) and p_1 , p_2 , p_3 , p_4 be the values of p at the ends of these legs By expressing p_1 , p_2 , p_3 , p_4 in terms of Taylor series expansions about the point (i,j) , Chan and Street (1970a) obtained

$$p_{ij} = \frac{\eta_1\eta_2\eta_3\eta_4}{2(\eta_2\eta_4 + \eta_1\eta_3)}\left[\frac{\eta_3 p_1 + \eta_1 p_3}{\eta_1\eta_3\left(\frac{\eta_1 + \eta_3}{2}\right)} + \frac{\eta_4 p_2 + \eta_2 p_4}{\eta_2\eta_4\left(\frac{\eta_2 + \eta_4}{2}\right)} + R_{ij}\right] \tag{15}$$

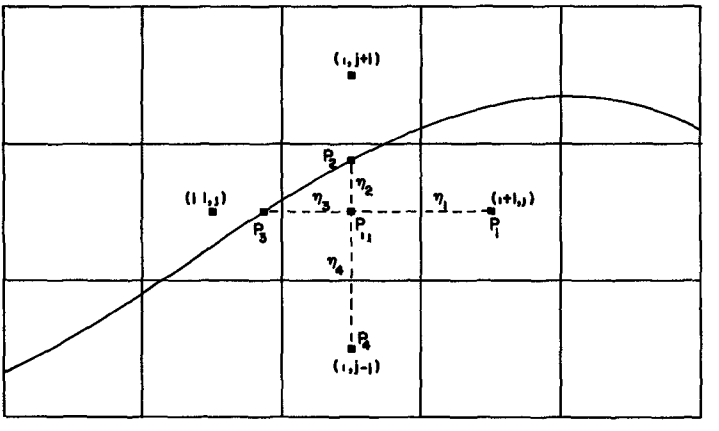

Fig 2 Irregular Star for P Calculations

A complete set of initial data -- the u and v fields and

the position of a line of particles depicting the free surface -- are needed to start the computation The initial pressure p need be known only approximately A hydrostatic distribution is adequate, because the p field is obtainable if u and v are given Chan and Street (1970b) described a method of generating the flow fields of a solitary wave which may be used as the initial condition in simulating the shoaling process

The evolution of the fluid dynamics is calculated in "cycles" or time steps At the start of each cycle the source term R_{ij} for each cell is evaluated by Eq (14) The pressure p is computed only for those cells whose centers fall within the fluid region Equation (12) is used if the centers of the four neighboring cells are all located on the fluid side of the free surface If any of these neighboring centers lies beyond the free surface, then Eq (15) is used The Successive Over-Relaxation method is employed to solve for p , with Eqs (12) and (15) being the iteration formulas The iteration is terminated when the condition

$$|p_{ij}^{(m)} - p_{ij}^{(m-1)}| < \varepsilon_p \tag{16}$$

is met for every cell, where (m) means the mth iteration and ε_p is a predetermined small positive number

Now we can compute the new velocities using Eqs (7) and (8) Then, each free surface marker particle is advanced to its new position by

$$x_k^{n+1} = x_k^n + u_k^{n+1}\,\delta t \ , \tag{17}$$

$$y_k^{n+1} = y_k^n + v_k^{n+1}\,\delta t \ , \tag{18}$$

where x_k and y_k refer to the position of the kth particle and the particle velocities u_k and v_k are interpolated from the velocity fields at the n+1th time step Thus, a cycle is completed and the next one can be immediately started

BOUNDARY CONDITIONS ON A SLOPE

A set of boundary conditions can be rigorously obtained for a plane beach of constant slope which coincides with the diagonal of the cells (Fig 3) The main consideration in deriving an equation for p_{ij} which lies on the beach face is the conservation of mass In Fig 3 we require that the net flow into the triangular region equal zero at the n+1th time step, viz ,

$$u^{n+1}_{i-\frac{1}{2}j}\,\delta y - v^{n+1}_{ij+\frac{1}{2}}\,\delta x = 0 \tag{19}$$

By substituting Eqs (7) and (8) into Eq (19) we have

$$P_{ij} = \frac{1}{Z_1}\left(\frac{P_{i-1j}}{\delta x^2} + \frac{P_{ij+1}}{\delta y^2} + R_{ij}\right) \tag{20}$$

where

$$Z_1 \equiv \frac{1}{\delta x^2} + \frac{1}{\delta y^2}\ , \tag{21}$$

$$R_{ij} \equiv \frac{1}{\delta t}\left(\frac{u^{*}_{i-\frac{1}{2}j}}{\delta x} - \frac{v^{*}_{ij+\frac{1}{2}}}{\delta y}\right) + \left(\frac{g_x}{\delta x} - \frac{g_y}{\delta y}\right) \tag{22}$$

In the iterative solution of the p field, Eq (20) is used at a beach cell

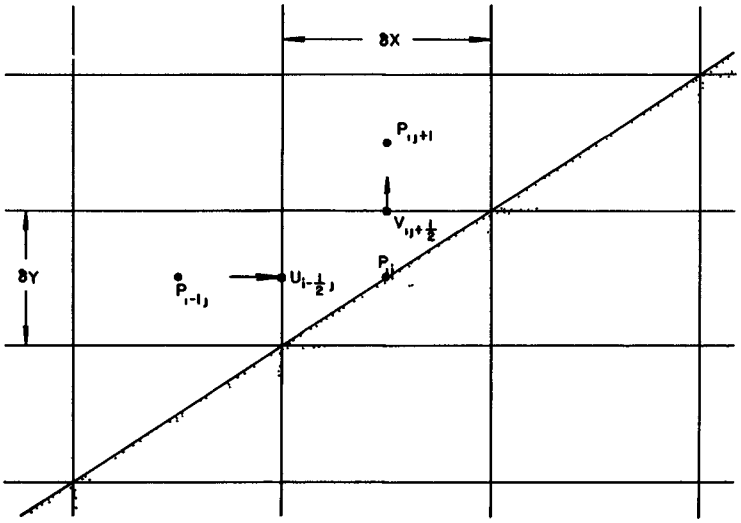

Fig 3 Definition Sketch for Computing p

Now, consider the diamond-shaped control volume for computing the convective contribution $u^*_{i+\frac{1}{2}j}$ (Fig 4) The total influx of the u-momentum is as follows

Through Face 1

$$M_1 = - \delta x \, v_{i+1j+\frac{1}{2}} \left(\frac{u_{i+\frac{1}{2}j} + u_{i+\frac{3}{2}j+1}}{2} \right) \tag{23}$$

Through Face 2

$$M_2 = \delta y \left(\frac{u_{i-\frac{1}{2}j} + u_{i+\frac{1}{2}j}}{2} \right)^2 - \delta x \left(\frac{v_{ij-\frac{1}{2}} + v_{ij+\frac{1}{2}}}{2} \right) \left(\frac{u_{i-\frac{1}{2}j} + u_{i+\frac{1}{2}j}}{2} \right) \tag{24}$$

Through Face 3

$$M_3 = \delta x \, v_{ij-\frac{1}{2}} \left(\frac{u_{i+\frac{1}{2}j} + u_{i-\frac{1}{2}j-1}}{2} \right) \tag{25}$$

Through Face 4

$$M_4 = \delta x \left(\frac{v_{i+1j-\frac{1}{2}} + v_{i+1j+\frac{1}{2}}}{2} \right) \left(\frac{u_{i+\frac{1}{2}j} + u_{i+\frac{3}{2}j}}{2} \right) - \delta y \left(\frac{u_{i+\frac{1}{2}j} + u_{i+\frac{3}{2}j}}{2} \right)^2 \tag{26}$$

The area of the control volume is $\delta x \delta y$ Therefore, by relating the net inflow of the u-momentum to its rate of increase, we obtain

$$\left(\frac{u^*_{i+\frac{1}{2}j} - u_{i+\frac{1}{2}j}}{\delta t} \right) (\delta x \delta y) = M_1 + M_2 + M_3 + M_4 \tag{27}$$

or, by rearranging,

$$u^*_{i+\frac{1}{2}j} = u_{i+\frac{1}{2}j} + \frac{\delta t}{\delta x \delta y} (M_1 + M_2 + M_3 + M_4) \tag{28}$$

The total $u^{n+1}_{i+\frac{1}{2}j}$ is then

$$u^{n+1}_{i+\frac{1}{2}j} = u^*_{i+\frac{1}{2}j} + \delta t \, g_x + \frac{\delta t}{\delta x} (p_{ij} - p_{i+1j}) \tag{29}$$

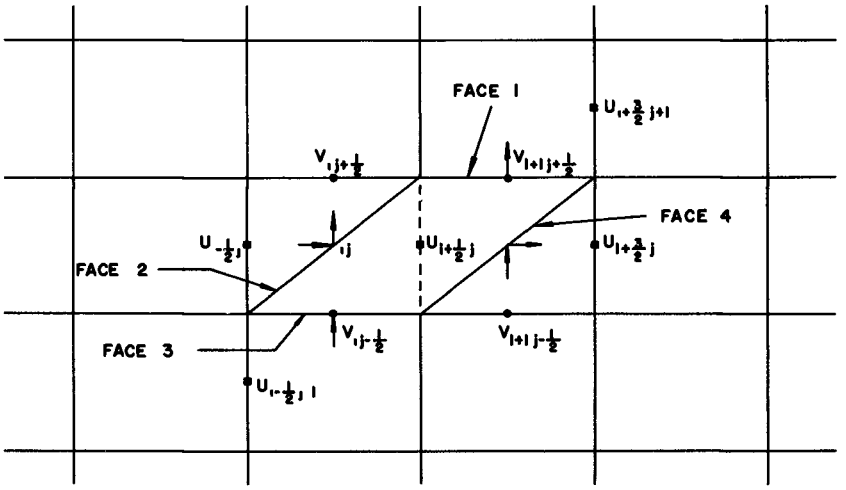

Fig 4 Definition Sketch for Computing u

If Face 4 is the beach face, then $M_4 = 0$ because there is no flow across it Similarly, we use $M_3 = M_4 = 0$ if both Face 3 and Face 4 are solid boundaries

To evaluate v^{n+1} near the beach face, a different type of diamond-shaped control volume is used (Fig 5) Again, the concept of balancing momentum within the control volume is employed to compute the convective contribution $v^*_{ij+\frac{1}{2}}$ The total influx of the v-momentum is as follows

Through Face 1

$$M_1 = - \delta y \, u_{i+\frac{1}{2}j+1} \left(\frac{v_{ij+\frac{1}{2}} + v_{i+1j+\frac{1}{2}}}{2} \right) \tag{30}$$

Through Face 2

$$M_2 = \delta y \left(\frac{u_{i-\frac{1}{2}j+1} + u_{i+\frac{1}{2}j+1}}{2} \right) \left(\frac{v_{ij+\frac{1}{2}} + v_{ij+\frac{3}{2}}}{2} \right) - \delta x \left(\frac{v_{ij+\frac{1}{2}} + v_{ij+\frac{3}{2}}}{2} \right)^2 \tag{31}$$

Through Face 3

$$M_3 = \delta y \, u_{i-\frac{1}{2}j} \left(\frac{v_{ij+\frac{1}{2}} + v_{i-1j-\frac{1}{2}}}{2} \right) \tag{32}$$

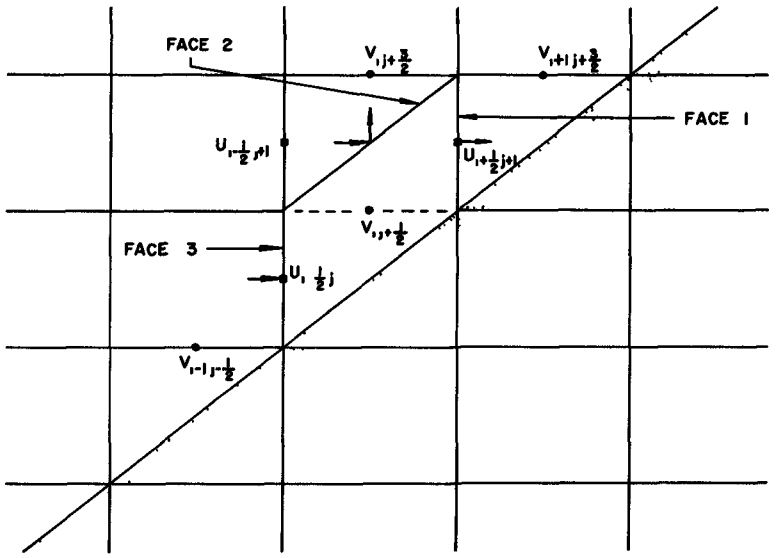

Fig 5 Definition Sketch for Computing v

Balancing the net inflow of the v-momentum with its rate of increase, we have

$$\left(\frac{v^*_{ij+\frac{1}{2}} - v_{ij+\frac{1}{2}}}{\delta t} \right) (\delta x \delta y) = M_1 + M_2 + M_3 \tag{33}$$

or

$$v^*_{ij+\frac{1}{2}} = v_{ij+\frac{1}{2}} + \frac{\delta t}{\delta x \delta y} (M_1 + M_2 + M_3) \tag{34}$$

The total $v^{n+1}_{ij+\frac{1}{2}}$ is then

$$v^{n+1}_{ij+\frac{1}{2}} = v^*_{ij+\frac{1}{2}} + \delta t \, g_y + \frac{\delta t}{\delta y} (p_{ij} - p_{ij+1}) \tag{35}$$

APPLICATION TO THE SHOALING OF WAVES

The initial position of the wave crest was chosen such that neither the left-hand wall nor the beach influenced the wave at $t = 0$. The beach slope used first was $S = 0.05$ (1 on 20). Each cell had the dimensions $\delta x = 0.50$ and $\delta y = 0.025$. The time increment was $\delta t = 0.05$. The initial wave height was $H_o = 0.25$.

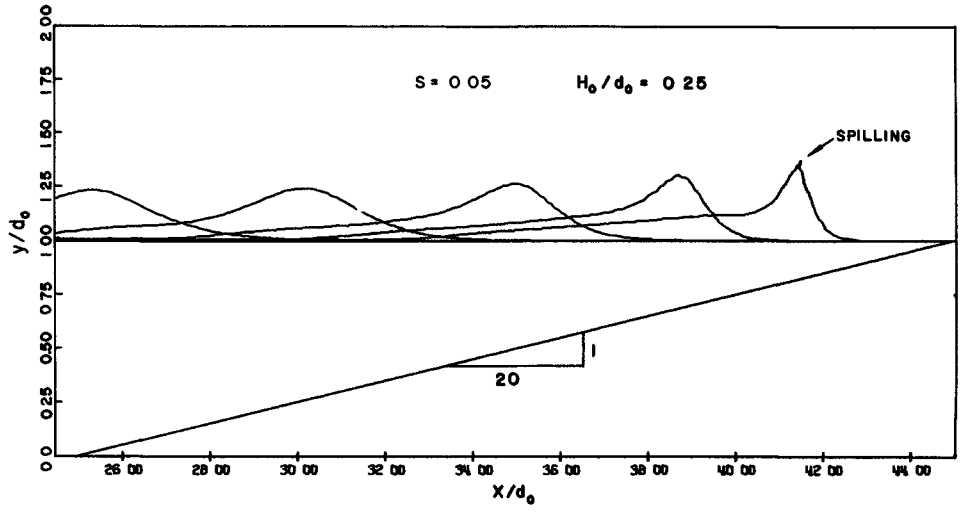

Fig. 6. Shoaling on a 1/20 Slope (Surface Profiles)

When the wave advances into the beach section where the water depth decreases, its shape changes. The wave profiles at various stages of shoaling are shown in Fig. 6. It is seen that the wave shape gradually loses symmetry on the beach. The wave has a steeper front than its hind part which looks like a long tail. At approximately $H/d = 2.0$, where H is the instantaneous wave height and d is the local still water depth under the wave crest, the wave crest peaks up with a very slight tendency to curl forward. This result is consistent with the observation of Ippen and Kulin (1955) that spilling rather than plunging occurs when a solitary wave of this magnitude breaks on the 1/20 slope. All these properties regarding the wave deformation also agree with the observations of Camfield and Street (1967).

The evolution of the fluid dynamics under the wave is best illustrated by the contour plots of the u and v fields. In Fig. 7(a) the time history of the distribution of u is shown. On the two outermost contour lines, $u = 0.015$. Then the value of u is

increased by 0 030 per line toward the wave crest Thus, u = 0 375 at the wave crest at t = 0 When the wave is well up the beach (t = 23 00) , u = 0 675 at its crest In Fig 7(b) the motion of the v field is shown To the left of the crest, the lowest contour line has v = -0.015 , and v decreases by 0 030 per line toward the free surface To the right of the crest, the lowest contour line has v = +0 015 , and v increases by 0 030 per line toward the free surface The line v = 0 lies between the lines v = ±0 015 and is not shown

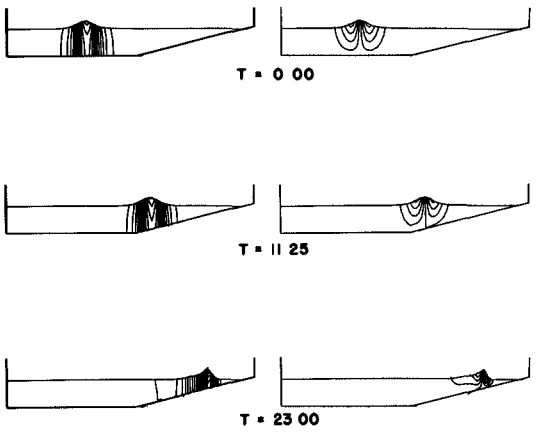

(a) u (b) v

Fig 7 Shoaling on a 1/20 Slope (Velocity Contours)

The contour lines in Fig 7 were computed by using a plotting program developed by Schreiber (1968) The facility used was an IBM 2250 graphic display device in which the computed contour lines are shown on a TV screen By directly photographing the surface of the screen, the contour plots were obtained Several motion pictures have also been made with this apparatus These graphical outputs prove to be valuable visual aids to an understanding of the physics in the waves

In Fig 8 the mass transport phenomenon in the mid-section of the beach is shown A vertical line of fluid particles are moved forward from their initial position x = 35 0 by the passing wave The mass transport here is of the translation-type as opposed to the oscillation-type in the periodic waves Also, the wave induced motion on the beach is seen to be quite uniform throughout the water depth

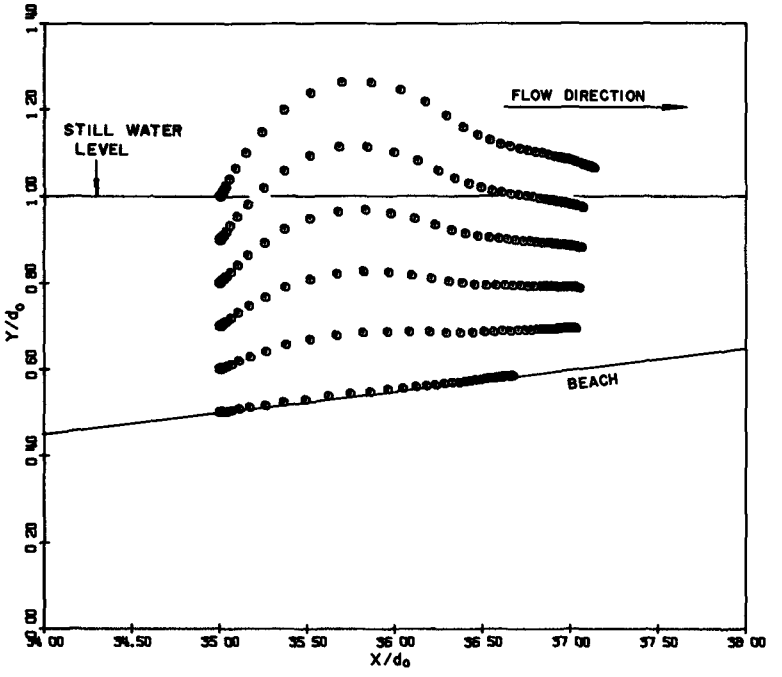

Fig 8 Shoaling on a 1/20 Slope (Particle Paths)

To study the growth of the wave height H as a function of the local water depth d , computations were conducted covering a range of the initial height-to-depth ratios (H_o/d_o) The results are compared with the experiments of Ippen and Kulin (1955) in Fig 9 Ippen and Kulin did not indicate the H_o/d_o value associated with each data point, but H_o/d_o is an important parameter in predicting the wave growth The scattering of the measured data cannot be reconciled without knowledge of this parameter However, the H_o/d_o ratio clearly has a profound effect on the wave's initial reaction to the slope Our results show that in the region $d/d_o > 0\ 45$, a solitary wave with smaller H_o/d_o has greater relative growth (H/H_o) The trend is reversed in the shallower region where $d/d_o < 0\ 45$ For $H_o/d_o = 0\ 10$ comparison was also made with the theories of Peregrine (1967), Madsen and Mei (1969) and the characteristics solution by Camfield and Street (1967) (Fig 10) With the exception of the characteristics solution, these theories seem to agree quite well

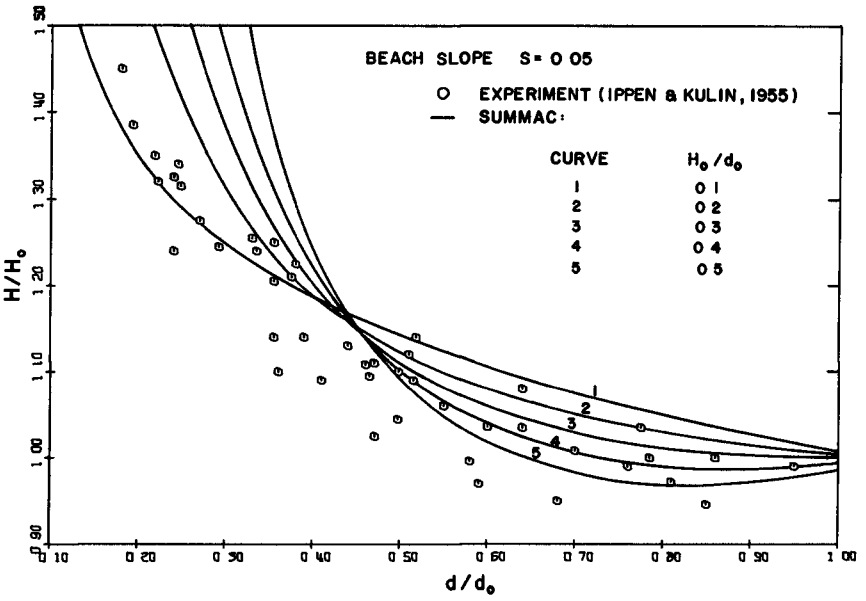

Fig 9 Growth of Wave Amplitude (S = 0 05)

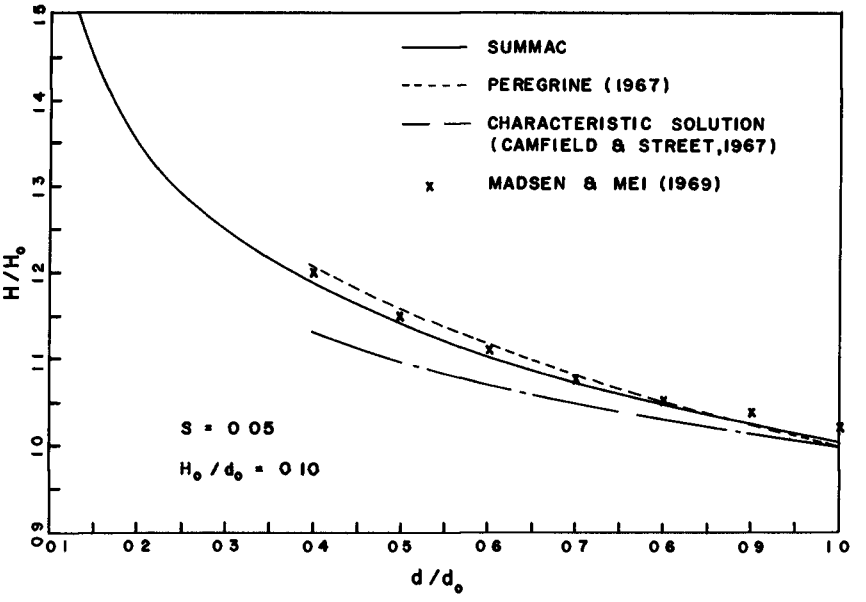

Fig 10 Comparison of Wave Amplitude Growth with Other Theories (S = 0 05)

Second, a wave with $H_o/d_o = 0\ 10$ was shoaled on a beach with $S = 0\ 045$ In Fig 11 the local height-to-depth ratio H/d is plotted against $x^*/d_b - 1/S$, where x^* is the distance measured from the intersection of the still water level and the beach and d_b ($\approx 0\ 085$) is the breaking depth The solution agrees favorably with the measurement of Camfield and Street (1967)

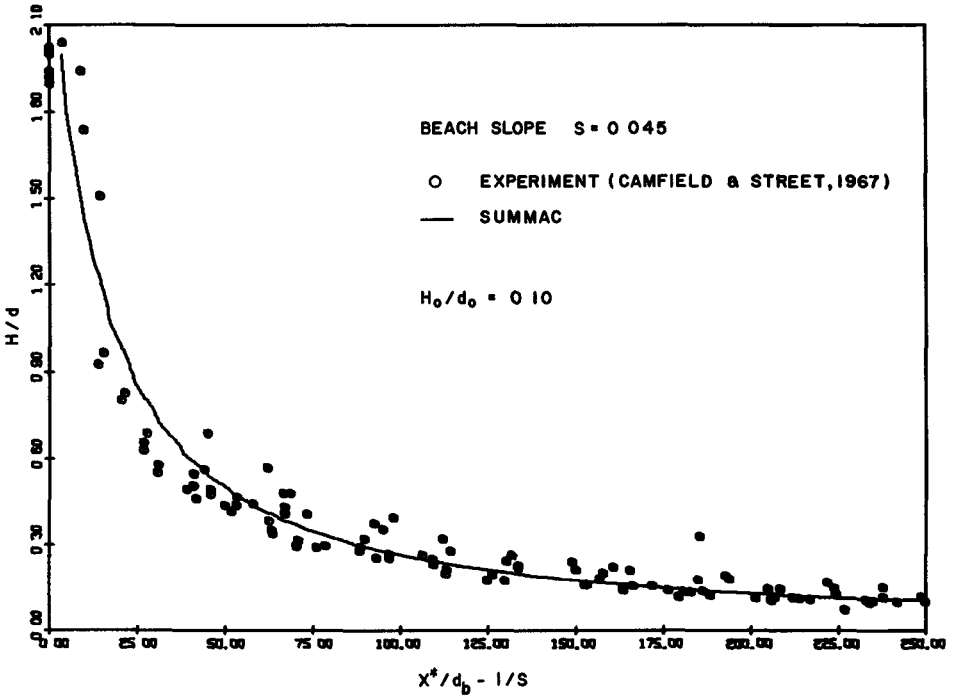

Fig 11 Growth of Wave Amplitude ($S = 0\ 045$)

We also simulated wave run-up on a 45° slope which has direct application to the study of wave run-up on coastline structures such as rubble-mound breakwaters The cell size was $\delta x = \delta y = 0\ 10$ The initial wave height was $H_o/d_o = 0\ 48$ and a time increment $\delta t = 0\ 05$ was used in computation The wave profiles at several stages of run-up are plotted in Fig 12 Quantitative comparison of these profiles with experiments was not made because of the difficulty in obtaining a computed profile which corresponds to a measured profile in time Nevertheless, the profiles closely resemble those observed by Street and Camfield (1966) We find the calculated envelope of the wave crests slightly higher than that of the experiment in the early stages of run-up, but the engineering interest is primarily in the prediction

of the maximum height of run-up R_o/d_o (Fig 12) The numerical model gave R_o/d_o = 1 27 which is equal to the measured value (Street and Camfield, 1966)

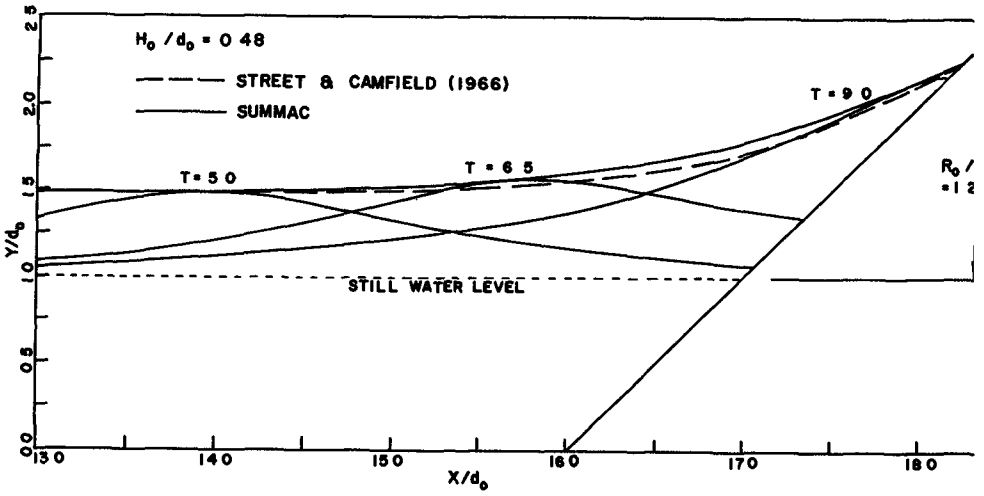

Fig 12 Run-up Profiles on a 45° Slope

CONCLUSIONS

The successful application of the SUMMAC technique to several physical problems indicates its usefulness as an engineering research tool for analyzing the dynamics of water waves in two space dimensions It is capable of providing accurate quantitative results as well as qualitative descriptions [e g , the prediction of wave run-up on a 45° slope] In addition, rapid advance in the design of high-speed computing systems makes numerical modeling economically feasible

While it is possible to employ the SUMMAC technique to attack a wide variety of water wave problems, some limitations inherent in the method must be noted First, as a result of achieving a high degree of accuracy in applying the free surface pressure condition by using irregular stars, waves after breaking cannot be simulated When breaking occurs, the computation must be terminated Second, only non-turbulent flows are considered in our model Although laminar viscous damping has little effect on large scale wave motions, energy dissipation due to the turbulence can be significant However, recent studies by Gawain and Pritchett (1970) and by Pritchett (1970) show that it is feasible to implement a phenomenological simulation of turbulence in the MAC framework

REFERENCES

Camfield, F E and Street, R L , Dept of Civil Engrg Tech Rept No 81, Stanford University, Calif (1967)

Chan, R K -C and Street, R L , Jour Computational Physics, 6, 1 (1970a)

Chan, R K -C and Street, R L , Dept of Civil Engrg Tech Rept No 135, Stanford University, Calif (1970b)

Dean, R G , Jour Geophysical Research, 70, 18 (1965)

Gawain, T H and Pritchett, J W , Jour Computational Physics, 6, 1 (1970)

Ippen, A T and Kulin, G , Dept of Civil and Sanitary Engrg Tech Rept No 15, Massachusetts Institute of Technology, Mass (1955)

Laitone, E V , Jour Fluid Mechanics, 9 (1960)

Lamb, Sir H , Hydrodynamics, Dover Publications (1945)

Madsen, O S and Mei, C C , Jour Fluid Mechanics, 39, 4 (1969)

Monkmeyer, P L and Kutzback, J E , Chapter 13, Coastal Engineering, Santa Barbara Specialty Conference, ASCE, New York (1965)

Peregrine, D H , Jour Fluid Mechanics, 27, 4 (1967)

Pritchett, J W , Information Research Asso., Inc , IRA-TR-1-70 (1970)

Schreiber, D E , IBM Research Report, RJ499, IBM Research Laboratory, San Jose, Calif (1968)

Stoker, J J , Water Waves, Interscience Publishers, Inc , New York (1957)

Street, R L and Camfield, F E , Dept of Civil Engrg Tech Note No 85(1)-66, Stanford University, Calif (1966)

Street, R L , Chan, R K -C , and Fromm, J E , 8th Symposium on Naval Hydrodynamics, CIT, Pasadena, Calif (1970)

Welch, J E , Harlow, F H , Shannon, J P , and Daly, B J , Los Alamos Scientific Lab Rept LA-3425 (1966)